J. DIFFERENTIAL GEOMETRY
31 (1990) 131-161

NUMERICAL ALGORITHMS FOR PROPAGATING INTERFACES: HAMILTON-JACOBI EQUATIONS AND CONSERVATION LAWS

J. A. SETHIAN

Abstract

In many physical problems, interfaces move with a speed that depends on the local curvature. Some common examples are flame propagation, crystal growth, and oil-water boundaries. We idealize the front as a closed, nonintersecting, initial hypersurface flowing along its gradient field with a speed that depends on the curvature. Because explicit solutions seldom exist, numerical approximations are often used. In this paper, we review some recent work on algorithms for attacking these problems. We show that algorithms based on direct parametrizations of the moving front face considerable difficulties. This is because such algorithms adhere to local properties of the solution, rather than the global structure. Conversely, the global properties of the motion can be captured by embedding the surface in a higher-dimensional function. In this setting, the equations of motion can be solved using numerical techniques borrowed from hyperbolic conservation laws. We apply the algorithms to a variety of complicated shapes, showing corner formation and breaking and merging, and conclude with a study of a dumbbell in R^3 moving under its mean curvature. We follow the collapsing dumbbell as the handle pinches off, a singularity develops, and the front breaks into two separate surfaces.

In many physical problems, interfaces move with speed that depends on the local curvature. Explicit solutions seldom exist. Thus, there is great interest in numerical algorithms that approximate the position of the moving front. In this paper, we review some recent work on algorithms for attacking these problems. The goal of this paper is to show that algorithms based on direct parametrizations of the moving front face considerable difficulties. This is because such algorithms adhere to local properties of the solution, rather than the global structure. Conversely, the

Received November 16, 1987 and, in revised form, July 8, 1988. This work is supported in part by the Applied Mathematics Subprogram of the Office of Energy Research under contract DE-AC03-76SF00098. The author also acknowledges the support of the National Science Foundation and the Sloan Foundation.

global properties of the motion are preserved by embedding the surface in a higher-dimensional function. In this setting, the resulting equations of motion can be accurately approximated by a new class of numerical techniques borrowed from hyperbolic conservation laws.

This paper is an expository review of techniques for approximating moving fronts. It is written for those who may be new to numerical analysis and computational algorithms for partial differential equations. The central ideas behind the hyperbolic conservation law approach were first presented in a paper by Osher and Sethian [24]. In that paper, the underlying theory, technical aspects of the algorithms, and applications were developed. The goal of this paper is to show the motivation behind this new class of algorithms and their application to problems of interest to geometers. Here, we will show why some algorithms work and others fail, and avoid technical discussions of higher order extensions and error analysis of convergence rates. The details of how to design and apply numerical algorithms based on the higher-dimensional Hamilton-Jacobi formulation to propagating fronts may be found in [24], and we refer the interested reader there.

We now state the problem. Suppose we are given a closed (or periodic), nonintersecting, initial hypersurface and a function $F(K)$. Here, K is the curvature of the hypersurface. We wish to compute the position of the surface as it flows along its gradient field with speed $F(K)$.

The outline of this paper is as follows. In §1, we describe two physical problems in which curvature plays a role in interface motion. In §2, we write down the equations of motion based on a parameterization of the moving front, and argue that numerical approximations to these equations face considerable difficulties. We show that a simple approximation to a moving initial cosine curve goes unstable with a very fine discretization of the parametrization, even though the exact solution stays smooth.

In §3, we take a global approach and view the $(N-1)$-dimensional moving surface as a level set of a time-dependent function of N space dimensions. The equation of motion for this function resembles an initial value Hamilton-Jacobi equation with parabolic right-hand side and is closely related to a viscous hyperbolic conservation law. We then show that numerical schemes designed to approximate hyperbolic conservation laws may be used to approximate the motion of the propagating surface. Finally, in §4, we apply our new schemes to a variety of propagation problems, demonstrating cusp formation, breaking and merging. We conclude with a new study of a dumbbell collapsing in R^3 under its mean curvature, and show the development of a singularity as the handle pinches off.

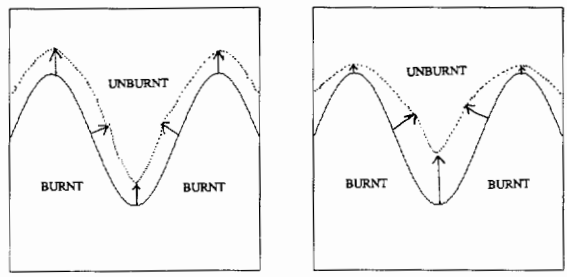

1a. Constant speed $F(K) = V$ 1b. Curvature dependence $F(K) = V(1 - \varepsilon K)$

FIGURE 1. Flame propagation: Speed dependent on curvature

1. Motivation

The first mathematical model of combustion was formulated by Landau [17] in 1944. He idealized a flame as an infinitely thin boundary separating regions of constant steady-state velocity, density, and temperature. In addition, he postulated that flames burn at a constant speed V normal to themselves. Under these assumptions, linear stability analysis showed that any deviation from an absolutely flat flame will become unbounded as time progresses. Numerous physical experiments indicate otherwise. In 1951, Markstein [21] argued that cool convex fingers reaching out into unburnt gas must propagate slower than hot concave regions surrounding an unburnt pocket. Thus, he proposed a curvature-dependent flame speed of the form $V(1 - \varepsilon K)$, where ε is a constant and K is the curvature. Here, $K > 0$ for convex fingers and $K < 0$ for concave fingers. Sketches of these ideas are shown in Figure 1. The addition of curvature stabilizes perturbations, and helps explain the formation of honey-combed "cellular flames" observed experimentally. More complicated flame models are discussed in [8], [22], [24], [31], [34].

In crystal growth, the dendritic spikes of a snowflake result, in part, from surface freezing rates which depend on curvature (see [18]). Consider a solid ice pellet growing in a supercooled liquid. The rate of growth at any point on the boundary depends on the curvature through the Gibbs-Thomson relation $T(\bar{x}) = T_M(1 - \varepsilon K(\bar{x}))$, where T_M is a constant melting temperature. Once again, $K > 0$ for convex fingers and $K < 0$ for concave fingers. In this case, the lower temperature of the extended fingers implies that they grow faster. Thus, the boundary breaks into separate dendrites

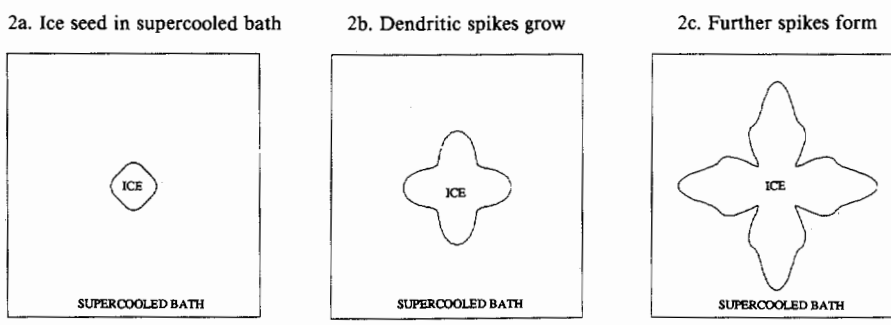

FIGURE 2. Crystal growth: Surface temperature dependent on curvature

which grow rapidly out from the seed and spawn further dendrites (see [3], [18], [19], [25], [33]. A qualitative picture is shown in Figure 2.

2. Lagrangian formulation: Equations and approximation

In this section, we derive equations of motion in terms of a parametrization of the moving front. For simplicity, we consider a closed curve moving in the plane. After some analysis, we study numerical schemes based on discrete approximations to these equations. A simple test problem shows the limitations of such schemes.

Equations of motion. Let $\gamma(0)$ be a smooth, closed initial curve in a Euclidean plane R^2. Let $\gamma(t)$ be the one-parameter family of curves generated by moving $\gamma(0)$ along its normal vector field with speed $F(K)$. Here, $F(K)$ is a given scalar function of the curvature K. The natural approach is to parametrize the moving curve. Let $\vec{x}(s,t)$ be the position vector which parametrizes γ at time t. Here, $0 \leq s \leq S$, and we prescribe periodic boundary conditions $\vec{x}(0,t) = \vec{x}(S,t)$. The curve is parametrized so that the interior is on the left in the direction of increasing s. Let $\vec{n}(s,t)$ be the outward normal and $K(s,t)$ be the curvature. Then $\vec{n} \cdot \vec{x}_t = F(K)$. In terms of individual components $\vec{x} = (x,y)$, we have

$$
\begin{aligned}
x_t &= F\left[\frac{y_{ss}x_s - x_{ss}y_s}{(x_s^2 + y_s^2)^{3/2}}\right]\left(\frac{y_s}{(x_s^2 + y_s^2)^{1/2}}\right), \\
y_t &= F\left[\frac{y_{ss}x_s - x_{ss}y_s}{(x_s^2 + y_s^2)^{3/2}}\right]\left(\frac{-x_s}{(x_s^2 + y_s^2)^{1/2}}\right).
\end{aligned} \tag{1}
$$

We call this a "Lagrangian" representation because the physical coordinate system moves with the front.

The special case of a closed curve shrinking under its own curvature has received considerable attention (see [7], [9], [10], [11], [14], [26]). Recently, it has shown that any smooth initial curve must collapse smoothly to a point if $F(K) = -K$ ([9], [10], [11], [14]). This result will be demonstrated for some complicated initial curves using the algorithms described in §3.

What happens to oscillations in the initial curve as it moves? We summarize the argument in [28] showing that the decay of oscillations depends only on the sign of F' at $K = 0$. Let $g(s,t) = (x_s^2 + y_s^2)^{1/2}$. Differentiating both sides of (1) with respect to s we obtain the evolution equations for the metric and curvature, namely

$$K_t = -g^{-1}(F_s g^{-1})_s - K^2 F, \tag{2}$$

$$g_t = gKF. \tag{3}$$

Denote the total oscillation in the propagating curve at time t by $\mathrm{Var}(t) = \int_0^S |K(s,t)| g(s,t)\, ds$. Suppose we have a nonconvex initial curve moving with speed $F(K)$, and suppose the moving curve stays smooth. Then it can be shown that $\frac{d}{dt}\mathrm{Var}(t) \leq 0$ if $F'(0) \leq 0$, and the inequalities can be made strict if $K_s(s,t) \neq 0$ whenever $K = 0$.

A simple test problem. Consider the speed function $F(K) = 1 - \varepsilon K$, where ε is a nonnegative constant. The curvature evolution equation becomes

$$K_t = \varepsilon K_{\alpha\alpha} + \varepsilon K^3 - K^2, \tag{4}$$

where we have changed variables and taken the derivative with respect to arclength α. (4) is a reaction-diffusion equation. The drive toward singularities due to the reaction term $(\varepsilon K^3 - K^2)$ is balanced by the smoothing effect of the diffusion term $(\varepsilon K_{\alpha\alpha})$. Indeed, with $\varepsilon = 0$, we have a pure reaction equation $K_t = -K^2$. In this case, the solution is $K(s,t) = K(s,0)/(1 + tK(s,0))$, which is singular at finite t if the initial curvature is anywhere negative. Thus, corners can form in the moving curve when $\varepsilon = 0$.

An example will serve as a test problem for our numerical schemes. Consider the periodic initial cosine curve

$$\gamma(0) = (-s, [1 + \cos 2\pi s]/2), \qquad -\infty < s < \infty, \tag{5}$$

propagating upward with speed $F(K) = 1 - \varepsilon K$, $\varepsilon > 0$. The troughs at $s = n + 1/2$, $n = 0, \pm 1, \pm 2, \cdots$, are sharpened by the negative reaction term (because $K < 0$ at such points) and smoothed by the positive diffusion term.

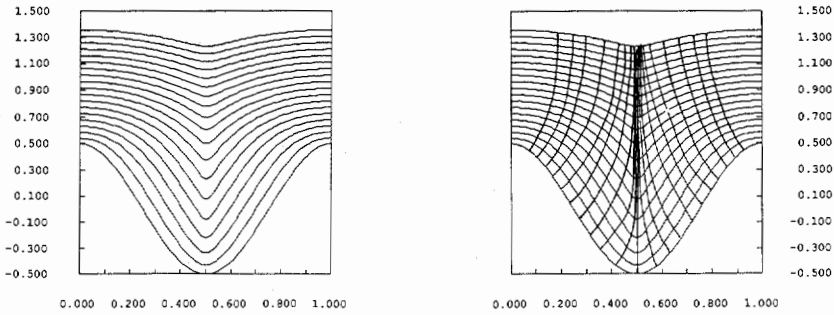

3a. $F(K) = 1 - \varepsilon K$, $\varepsilon = .01$

3b. Lines of constant parametrization superimposed on front

FIGURE 3. Exact solution: Propagating initial cosine curve

Do corners develop in the moving front? For small initial times, the reaction term is stronger than the diffusion term, and the troughs begin to sharpen and close. By the argument above, we know that for $\varepsilon = 0$, a corner must form. On the other hand, for $\varepsilon > 0$, it can be shown (see [24], [28] and §3), that the moving front stays C^∞. Thus, we can use an extension of the previous statement on decay of oscillations to periodic initial curves and the fact that $F'(K) = -\varepsilon < 0$ to show that $d\,\mathrm{Var}(t)/dt < 0$. Hence, peaks and valleys in the moving curve must decay.

The propagating curve is shown at various times in Figure 3a. The front becomes flat as t increases. In Figure 3b, we superimpose lines of constant s. The fact that s does not correspond to arclength is evident in the narrowing of constant parameter lines at the trough. In the next section, we show that this poses considerable difficulty for numerical approximation schemes.

Numerical approximations to Lagrangian formulation. Two key issues for any numerical scheme are accuracy and stability. The *accuracy* of a scheme determines how well the discrete formulation approximates the exact equation. *Stability* measures how sensitive the approximation is to small deviations. In this section, we argue that the stability requirement for Lagrangian schemes forces an unreasonably small time step.

We construct a very simple difference approximation to the Lagrangian equations of motion. Divide the parametrization interval $[0, S]$ into M equal intervals of size Δs, yielding $M + 1$ mesh points $s_i = i\Delta s$, $i = 0, \cdots, M$. Divide time into equal intervals of length Δt. The image of

each mesh point $i\Delta s$ at each time step $n\Delta t$ is a marker point (x_i^n, y_i^n) on the moving front. Our goal is a *numerical algorithm* which produces new values $(x_i^{n+1}, y_i^{n_1+1})$ from the previous positions. First, we approximate parameter derivatives at each marker point by using neighboring mesh points. The *central difference approximations* based on Taylor series are given by

$$(6) \qquad (x_i^n)_s \approx \frac{x_{i+1}^n - x_{i-1}^n}{2\Delta s}, \qquad (y_i^n)_s \approx \frac{y_{i+1}^n - y_{i-1}^n}{2\Delta s},$$

$$(7) \qquad (x_i^n)_{ss} \approx \frac{x_{i+1}^n - 2x_i^n + x_{i-1}^n}{\Delta s^2}, \qquad (y_i^n)_{ss} \approx \frac{y_{i+1}^n - 2y_i^n + y_{i-1}^n}{\Delta s^2}.$$

Similarly, time derivatives may be replaced by *forward difference approximations*

$$(8) \qquad \frac{dx_i^n}{dt} \approx \frac{x_i^{n+1} - x_i^n}{\Delta t}, \qquad \frac{dy_i^n}{dt} \approx \frac{y_i^{n+1} - y_i^n}{\Delta t}.$$

Substituting these approximations into the equations of motion (Equation (1)), we get

$$(9) \qquad (x_i^{n+1}, y_i^{n+1}) = (x_i^n, y_i^n) + \Delta t \frac{F(K_i^n)}{((x_{i+1}^n - x_{i-1}^n)^2 + (y_{i+1}^n - y_{i-1}^n)^2)^{1/2}} \cdot (y_{i+1}^n - y_{i-1}^n, -(x_{i+1}^n - x_{i-1}^n)),$$

$$(10) \qquad \begin{aligned} K_i^n = {} & 4[(x_{i+1}^n - x_{i-1}^n)^2 + (y_{i+1}^n - y_{i-1}^n)^2]^{-3/2} \\ & \cdot [(y_{i+1}^n - 2y_i + y_{i-1}^n)(x_{i+1}^n - x_{i-1}^n) \\ & - (x_{i+1}^n - 2x_i + x_{i-1}^n)(y_{i+1}^n - y_{i-1}^n)]. \end{aligned}$$

Using the periodicity of the curve, this is a complete recipe for updating the positions of the particles from one time step to the next.

We observe that the fixed discretization interval Δs has dropped out of the above expression. Consequently, as marker particles come together, quotients in the right-hand side of (9) approach zero over zero. This is a very sensitive calculation. The computed curvature can change drastically from one particle to the next because of small and unavoidable errors in the positions.

We can demonstrate this unstable growth of small errors by using our scheme to follow the initial cosine curve. Since $\varepsilon > 0$, the exact solution is always smooth. We use 50 marker points and time step $\Delta t = 0.01$. Although the propagating front begins to sharpen as expected (see Figure 4a), oscillations soon develop which grow uncontrollably. These oscillations result from a feedback cycle: (1) small errors in approximate marker

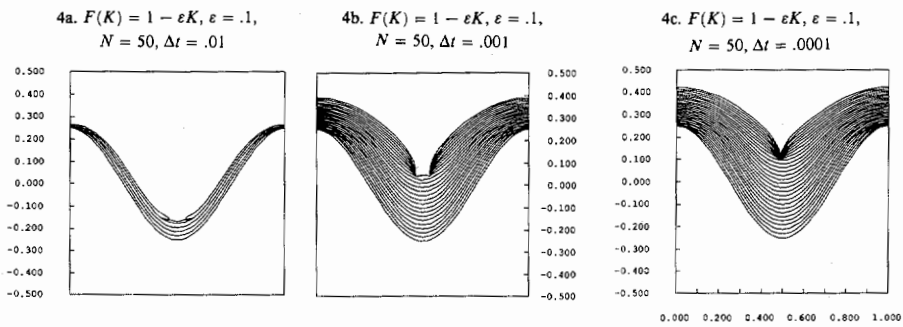

FIGURE 4. Marker particle approximation of propagating initial cosine curve

positions produce (2) local variations in the computed derivatives leading to (3) variation in the computed particle velocities causing (4) uneven advancement of markers which yields (5) larger errors in approximate marker positions. Within a few time steps, the small oscillations in the curvature have grown wildly and the computed solution becomes unbounded. In Figure 4a, we show the calculation until the computer program stops running, due to overflow.

Suppose we try to increase accuracy by using a smaller time step. In Figures 4b and 4c, we show calculations with $\Delta t = .001$ and $\Delta t = .0001$, respectively. Once again, the solution becomes unstable, and the smooth decay of the trough is not seen. It is important to point out that for any $\varepsilon > 0$, there is a bound for the minimum distance between particles. Thus, a small enough time step does exist to insure stability. The issue here is *practicality*. Such a time step may be so unreasonably small that the calculation simply takes too long. The larger ε, the larger a time step may be chosen without violating stability. However, in the limiting case $\varepsilon = 0$, the equations reduce to a linearly unstable hyperbolic system (see [24]). In this case, marker particle solutions along characteristic *must* go unstable.

Two remedies are often proposed to circumvent these problems. One option is to "smooth" the speed function $F(K)$ so that constant parameter curves stay far enough apart. Another option is to redistribute marker particles according to arclength every few time steps. Both options are designed to produce a practical time step that maintains stability.

Ultimately, serious difficulties remain. With both remedies, the equations have been altered in nonobvious ways. Significant amounts of

smoothing of the speed function may be required to insure a practical time step. Thus, one has chosen to sacrifice the most interesting propagation characteristics, such as front sharpening and curvature singularities, in order to keep the calculation alive. Similarly, calculation of arclength adds an additional smoothing term to the speed function and is difficult to analyze. Due to these two effects, the computed solution may be far from the desired one. In the worst case, time and effort are spent solving an unrelated problem.

Topological changes in the moving front are also problematic for Lagrangian approximation schemes. Consider two separate regions of growing substance in a plane, each surrounded by a closed curve. Suppose these patches merge and the boundary becomes a single curve. It is difficult to produce a systematic way of removing those markers that no longer sit on the actual boundary. The bookkeeping of removing, redistributing, and connecting markers becomes even more complicated for higher dimensional interface problems.

To summarize, Lagrangian approximations suffer from instability and topological limitations because they follow a local representation of the front. In the next section, we take a global approach.

3. Eulerian formulation: Equations and approximations

In this section, we repeat the derivation presented in [24] and reformulate the problem, showing a link between the resulting Hamilton-Jacobi equation and a hyperbolic conservation law. We then show that the central difference approximation fails, because it ignores a global "entropy condition" which applies when sharp corners develop. Finally, we compute the motion of the propagating cosine curve using the simplest possible entropy-satisfying algorithm.

Equations of motion. We will motivate our approach with a simple example. Suppose the initial front γ at $t = 0$ is a circle in the xy-plane (Figure 5a). We imagine that the circle is the level set $\psi = 0$ of an initial surface $z = \psi(x, y, t = 0)$ in R^3 (see Figure 5b). We can then match the one-parameter family of moving curves $\gamma(t)$ with a one-parameter family of moving surfaces in such a way that the level set $\psi = 0$ always yields the moving front (Figures 5c, 5d). All that remains is to find an equation of motion for the evolving surface.

In the general case, let $\gamma(0)$ be a closed, nonintersecting, $(N-1)$ dimensional hypersurface. Let $\psi(\bar{x}, t)$, $\bar{x} \in R^n$, be the scalar function such that $\psi(\bar{x}, 0) = \pm d(\bar{x})$, where $d(\bar{x})$ is the signed distance from $\bar{x}$ to the

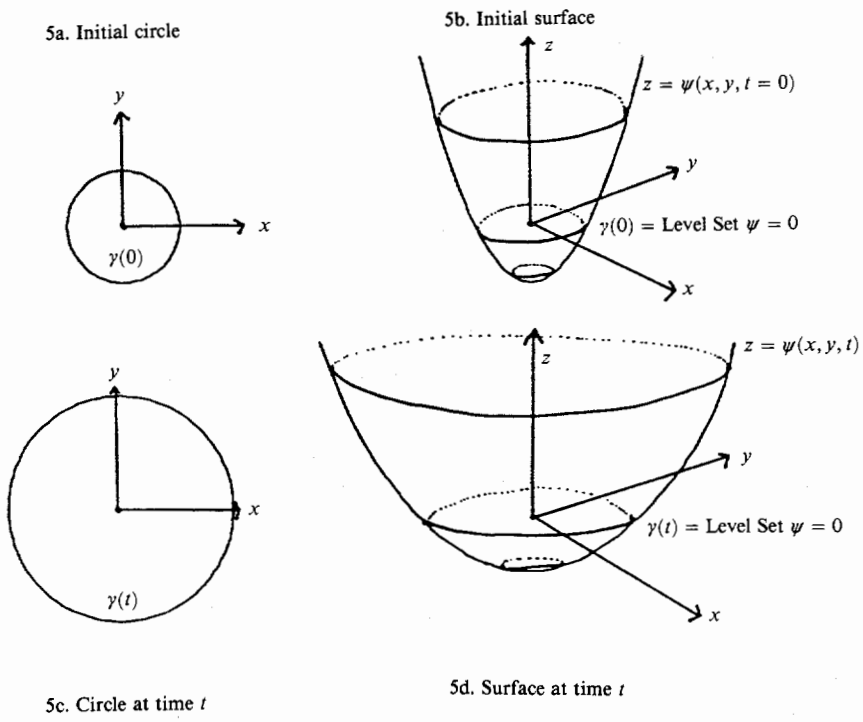

FIGURE 5. Eulerian formulation of equations of motion

hypersurface $\gamma(0)$. We use the plus sign if $\bar{x}$ is outside $\gamma(0)$ and the minus sign if $\bar{x}$ is inside. Each level set of ψ flows along its gradient field with speed $F(K)$. The gradient $\nabla\psi(\bar{x}, t)$ is normal to the $(N-1)$-dimensional level set passing through $\bar{x}$. Let $K(\bar{x}, t)$ be the curvature of that level set at $\bar{x}$. We may then express K in terms of ψ. For example, if $\bar{x} \in R^2$, then $K \equiv (\psi_{yy}\psi_x^2 - 2\psi_x\psi_y\psi_{xy} + \psi_{xx}\psi_y^2)/(\psi_x^2 + \psi_y^2)^{3/2}$. In higher dimensions, appropriate expressions may be obtained for the mean curvature or for the Gaussian curvature. Thus, the motion of each level set is given by

$$\psi_t + F(K)|\nabla\psi| = 0. \tag{11}$$

At any time, the moving front $\gamma(t)$ is just the level set $\psi = 0$.

We call this an *Eulerian formulation* for front propagation, because it is written in terms of a fixed coordinate system in the physical domain. There are three advantages to this approach. First, since the underlying coordinate system is fixed, discrete mesh points do not move and the stability problems that plagued the Lagrangian approximations may be avoided.

Second, topological changes are handled naturally, since the level surface $\psi = 0$ need not be simply connected. Third, it clearly works in any number of space dimensions.

Hamilton-Jacobi equations and hyperbolic conservation laws. Consider the typical speed function $F(K) = 1 - \varepsilon K$. The equation of motion

$$\psi_t + |\nabla\psi| = \varepsilon K|\nabla\psi| \tag{12}$$

is reminiscent of a broad class of equations known as "Hamilton-Jacobi equations with viscosity" (see [4]). The left-hand side is the Hamilton-Jacobi equation part, and the "viscosity" refers to the second-order "parabolic-like" right-hand side.

Assume the moving front is a curve in two space dimensions that remains a graph and consider the initial front given by the graph of $f(x)$, with f and f' periodic on $[0, 1]$. Let ϕ be the height of the propagating function at time t, thus $\phi(x, 0) = f(x)$. The normal at (x, ϕ) is $(1, \phi_x)$, and the equation of motion becomes $\phi_t = F(K)(1 + \phi_x^2)^{1/2}$. Using the speed function $F(K) = 1 - \varepsilon K$ and the formula $K = -\phi_{xx}/(1 + \phi_x^2)^{3/2}$, we get

$$\phi_t - (1 + \phi_x^2)^{1/2} = \varepsilon \frac{\phi_{xx}}{1 + \phi_x^2}. \tag{13}$$

Suppose we now try to construct an evolution equation for the slope $u = d\phi/dx$ of the propagating front. Differentiating both sides of the above with respect to x and substituting, we get

$$u_t + [-(1 + u^2)^{1/2}]_x = \varepsilon \left[\frac{u_x}{1 + u^2}\right]_x. \tag{14}$$

Thus, the derivative of the Hamilton-Jacobi equation with parabolic right-hand side for the changing height ϕ is a viscous hyperbolic conservation law for the propagating slope u (see [24]).

Much is known about hyperbolic conservation laws, (see [5], [6], [12], [20], [23]). For $\varepsilon > 0$, the parabolic right-hand side diffuses steep gradients and enforces smooth solutions (this is the main fact underlying these statements in §2). However, for $\varepsilon = 0$, discontinuous solutions can arise from smooth initial data. A variety of weak solutions which satisfy an integral version of (14) are possible beyond the occurrence of the singularity. Of all such weak solutions, we are interested in the one that is the limit of smooth solutions as $\varepsilon \to 0$. This particular weak solution can be selected with the help of a so-called entropy condition.

We now illustrate these ideas by studying our propagating cosine curve. We have already seen that with $\varepsilon > 0$, the exact solution develops a sharpening trough which ultimately stays smooth. On the other hand, for $\varepsilon = 0$

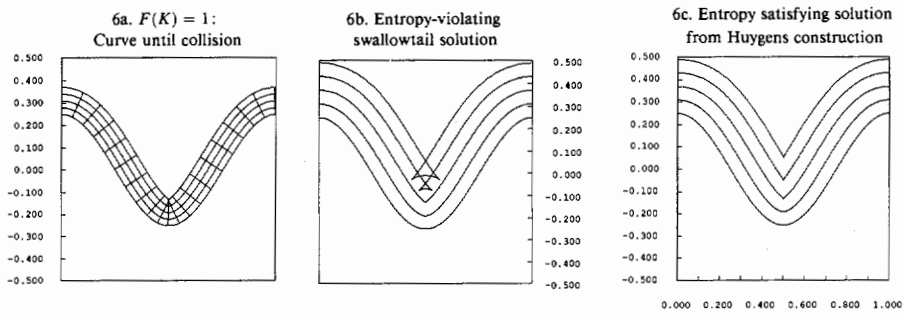

FIGURE 6. Formation of corner and weak solutions for constant speed case

a corner must develop (see Figure 6a). Thus, jump discontinuities in the slope arise from smooth initial data. How do we proceed once a corner develops? It is unclear how to construct the normal at the corner and continue the evolution, since the derivative is not defined there. One possibility is the "swallowtail" solution formed by letting the front pass through itself (see Figure 6b). However, from a geometrical argument it seems clear that the front at time t should consist of only the set of all points located a distance t from the initial curve. (This is known as the Huygens principle construction; see [3].) Roughly speaking, we want to remove the "tail" from the "swallowtail". In Figure 6c, we show this alternate weak solution. Another way to characterize this weak solution is through the following "entropy condition" (see [27]): If the front is viewed as a burning flame, *then once a particle is burnt it stays burnt.* Careful adherence to this stipulation produces the Huygens principle construction. Furthermore, this physically reasonable weak solution has an equally appealing mathematical quality: It is the formal limit of the smooth solutions $\varepsilon > 0$ as the curvature term vanishes (see [24], [28], [30]).

An unsuccessful calculation. Perhaps the most straightforward way of creating an algorithm to approximate the solution to (13) is to replace all spatial derivatives with central differences and the time derivative with a forward difference, just as we did in (9) and (10). In this section, we show why such an algorithm may not work. Let $F(K) = 1$ and consider the initial value problem

$$\phi_t = (1 + \phi_x^2)^{1/2}, \tag{15}$$

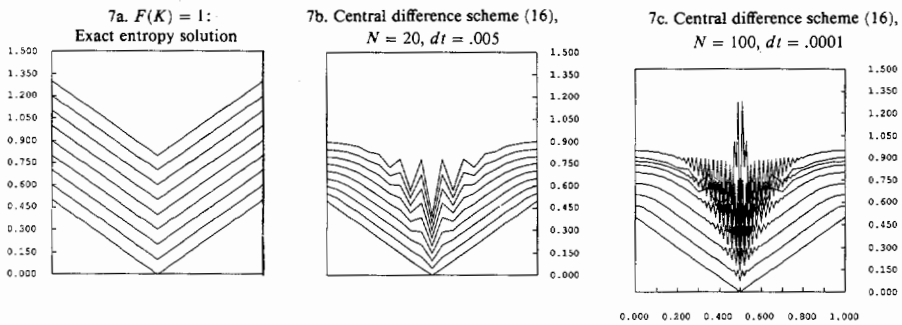

FIGURE 7. Blow-up of central difference approximation

$$\phi(x,0) = f(x) = \left\{ \begin{matrix} (1/2 - x), & x \le 1/2 \\ (x - 1/2), & x > 1/2 \end{matrix} \right\}.$$

The initial front is a "V" formed by rays meeting at $(1/2, 0)$. By our entropy condition, the solution at any time t is the set of all points located a distance t from the initial "V" (see Figure 7a). Divide the interval $[0, 1]$ into $2M - 1$ points, and form the central difference approximation to the spatial derivative ϕ_{xx} in (15), namely

$$\frac{\phi_i^{n+1} - \phi_i^n}{\Delta t} = \left[1 + \left(\frac{\phi_{i+1}^n - \phi_{i-1}^n}{2\Delta x} \right)^2 \right]^{1/2}. \tag{16}$$

(We postpone for a moment replacing the time derivative.) Since $x_M = 1/2$, by symmetry, $\phi_{M+1} = \phi_{M-1}$, thus $\phi_t(1/2, 0) = 1$. However, for all $x \neq 1/2$, ϕ_t is correctly calculated to be $\sqrt{2}$, since the graph is linear on either side of the corner and thus the central difference approximation is exact. Note that this has nothing to do with the size of the space step Δx or the time step Δt. *No matter how small we take the numerical parameters, the approximation to ϕ_t at $x = 1/2$ get no better.* It is simply due to the way in which the derivative ϕ_x is approximated. In Figures 7b and 7c, we show results using this scheme, with the time derivative ϕ_t replaced by a forward difference scheme.

It is easy to see what has gone wrong. In the exact solution (Figure 7a), $\psi_t = \sqrt{2}$ for all $x \neq 1/2$. This should also hold at $x = 1/2$ where the slope is not defined; the Huygens construction sets $\psi_t(x = 1/2, t)$ equal to $\lim_{x \to 1/2} \psi_t$. Unfortunately, the central difference approximation chooses a different (and, for our purpose, wrong) limiting solution. It sets the

undefined slope ψ_x equal to the average of the left and right slopes. As the calculation progresses, this miscalculation of the slope propagates outwards from the spike as wild oscillations, as may be seen by examining the scheme in detail. Eventually, these oscillations cause blowup in the code. It is clear that some more care must be taken in formulating an algorithm.

Stable, consistent, entropy-satisfying algorithms. The entropy condition for propagating fronts is identical to the one for hyperbolic conservation laws, where stable, consistent, entropy-satisfying numerical algorithms have a rich history. The most effective schemes have resulted from a combination of partial differential equations theory, numerical analysis, physical intuition, computing experience, and clever fine tuning (see [5], [6], [13], [32]). In this section, we give a simple first order algorithm which transforms into an effective algorithm for our moving front problems. Unlike the above central difference approximation, this scheme will "smear out" sharp corners in such a way that the algorithm approximates the correct solution.

A single, nonlinear equation of the form

$$u_t + [H(u)]_x = 0 \tag{17}$$

is called a *hyperbolic conservation law.* (14) for the propagating slope $u = \phi_x$ is a conservation law in the limiting case $\varepsilon = 0$ with $H(u) = -(1+u^2)^{1/2}$. Since the propagating front can develop corners, we know that discontinuities may develop in the slope u from smooth initial data. Thus, we study an integral version of the conservation law which admits discontinuous solutions. Consider a closed interval $[a, b]$. We may integrate both sides of (17) to produce

$$\frac{d}{dt}\int_a^b u(x,t)\,dx = H[u(a,t)] - H[(b,t)]. \tag{18}$$

We say that u is a weak solution of the conservation law if it satisfies the above integral equation. Note that u need not be differentiable to satisfy the integral form of the conservation law. The smoothness issue is circumvented by devising numerical algorithms to approximate the integral rather than differential equation of motion.

Definition. Let u_i^n be the value of u at mesh point $i\Delta x$ at time $n\Delta t$. We say that a 3-point difference scheme is in *conservation form* ([13], [20]) if there exists a function $g(u_1, u_2)$ such that the scheme can be written in the form

$$\frac{u_i^{n+1} - u_i^n}{\Delta t} = -\frac{g(u_i^n, u_{i+1}^n) - g(u_{i-1}^n, u_i^n)}{\Delta x}, \quad \text{where } g(u,u) = H(u). \tag{19}$$

This definition is natural; the scheme must approximate the hyperbolic conservation law, subject to the consistency requirement $g(u,u) = H(u)$. Thus, any scheme that can be put into conservation form gives a weak solution. But how do we guarantee that the scheme picks out the correct entropy-satisfying weak solution? We must restrict things further. We say that a 3-point finite difference scheme of the form $u_i^{n+1} = F(u_{i-1}^n, u_i^n, u_{i+1}^n)$ is *monotone* if F is an increasing function of all its arguments. We now can state the main fact (see [32]): A conservative, monotone scheme produces a solution that satisfies the entropy condition. Thus, we need only check monotonicity and conservation form to verify that a scheme gives the correct entropy condition. One such simple scheme, called the Lax-Friedrichs method [20], is built from central difference approximations and given by

$$u_i^{n+1} = \frac{1}{2}(u_{i-1}^n, u_{i+1}^n) - \frac{\Delta t}{\Delta x}[H(u_{i+1}^n)]. \tag{20}$$

It is straightforward to verify that this scheme is monotone and may be put in conservation form via the numerical flux function

$$g(u_1,u_2) = -\frac{\Delta x}{2\Delta t}(u_2 - u_1) + \frac{1}{2}[H(u_2) + H(u_1)]. \tag{21}$$

With the additional constraint that $\Delta t/\Delta x < 1$, this scheme provides a straightforward way of approximating the solution to (17).

How do we go from a scheme for the slope u to a scheme for the front ϕ itself? One simple idea is to solve for u and integrate. However, there is another, even easier, way. In the limiting case $\varepsilon \to 0$, we may rewrite the front propagation equation as $\phi_t + H(d\phi/dx) = 0$, where $H(u) = -(1+u^2)^{1/2}$. Using a forward difference scheme in time, we have $\phi_i^{n+1} = \phi_i^n - \Delta t H(u)$. Since our numerical flux function g approximates H, we can write

$$\phi_i^{n+1} = \phi_i^n - \Delta t\, g((\phi_i^n - \phi_{i-1}^n)/dx, (\phi_{i+1}^n - \phi_i^n)/dx), \tag{22}$$

where g is defined above. This algorithm produces the correct entropy-satisfying weak solution, and will be used to propagate our initial cosine curve. Finally, if $\varepsilon \neq 0$, we may use a straightforward finite difference scheme to approximate spatial derivatives for the parabolic curvature-dependent right-hand side.

These ideas may be extended to produce entropy-satisfying algorithms for the full Eulerian equations of motion given in (11) (see [24]). One further point should be made. It is advantageous to use *upwind schemes* which calculate derivatives in the direction of the outward flowing normals. If such schemes are used, necessary numerical boundary conditions far

from the region of interest do not flow backwards and create spurious solutions. One of the most straightforward and effective upwind schemes is the Engquist-Osher scheme ([5], [6], [24]). In the next section, we show the application of this upwind scheme to a variety of hypersurface propagation problems.

4. Examples

In this section, we show the application of our entropy-satisfying, upwind algorithm to the motion of a collection of test problems. Many of these examples are discussed in detail in [24]. In these examples, the input parameters are the initial position of the hypersurface, the time step Δt, the number of grid points in each coordinate direction, and the particular speed function $F(K)$. Formation of cusps, generation of the entropy-satisfying weak solution, and changes in topology (merging and breaking) are handled automatically by the Hamilton-Jacobi formulation.

Propagating initial cosine curve: $F(K) = 1 - \varepsilon K$. We first demonstrate the diffusive effects of curvature on the formation of singularities in the propagating front. We consider an initial cosine curve $\gamma(0) = \cos(8\pi x)$, $0 \leq x \leq 1$, propagating with speed $F(K) = 1 - \varepsilon K$. Periodic boundary conditions are employed at $x = 0$ and $x = 1$. We use 160 mesh points and time step $\Delta t = .001$. Because the moving front always remains the graph of a function, we solve the Hamilton-Jacobi with viscosity equation given in (13). In Figure 8, we graph the front at various times. In the case $\varepsilon = 0$ (Figure 8a), corners form in the moving front, and these curvature singularities propagate upwards. In the case $\varepsilon = 0.025$ (Figure 8b), the front stays smooth due to the diffusive curvature term. In the case $\varepsilon = 0.1$ (Figure 8c), diffusion is so large ($1 - \varepsilon K < 0$) that the peaks first move down before they flatten out enough to propagate upwards. These calculations were difficult to perform using the marker particle Lagrangian representation of §2, even with an order of magnitude more smoothing ($\varepsilon = 0.1$ compared with $\varepsilon = 0.01$ here).

Star-shaped front burning out: $F(K) = 1$. We consider a seven-pointed star

$$\gamma(0) = (0.1 + (0.065)\sin(7 \cdot 2\pi s))(\cos(2\pi s), \sin(2\pi s)), \qquad 0 \leq s \leq 1,$$

as the initial curve and solve the Hamilton-Jacobi level set formulation (11). We choose speed function $F(K) = 1$ and view the boundary as a flame burning outwards. The computational domain is a square centered at the origin of side length 1/2. We use 300 mesh points per side and

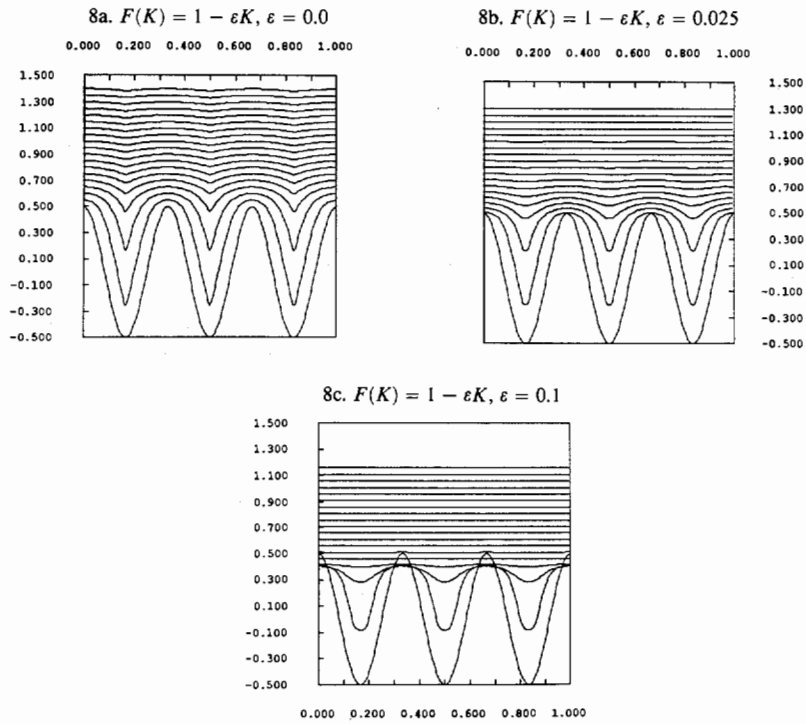

All plots at $T = 0.0, 0.9\ (0.05)$

FIGURE 8. Propagating initial cosine curve: $F(K) = 1 - \varepsilon K$. (Reprinted from [24])

a time set $\Delta t = .0005$. We follow an entire family of concentric star-shaped curves moving on the higher-dimensional surface $\psi(x, y, t)$. At any time $n\Delta t$, the front is plotted by passing the discrete grid function Ψ_{ij}^n to a standard contour plotter and asking for the contour $\Psi = 0$. The initial curve corresponds to the boundary of the shaded region, and the position of the front at various times is shown in Figure 9. The smooth initial curve develops sharp corners which then open up at the front burns, asymptotically approaching a circle.

Spiral collapsing under curvature: $F(K) = -K$. In this example, we let $F(K) = -K$, corresponding to a front moving in with speed equal to its curvature. It has recently been shown ([9], [10], [11], [14]) that any nonintersecting curve must collapse smoothly to a circle under this motion. In Figure 10, we show the results of this motion applied to the

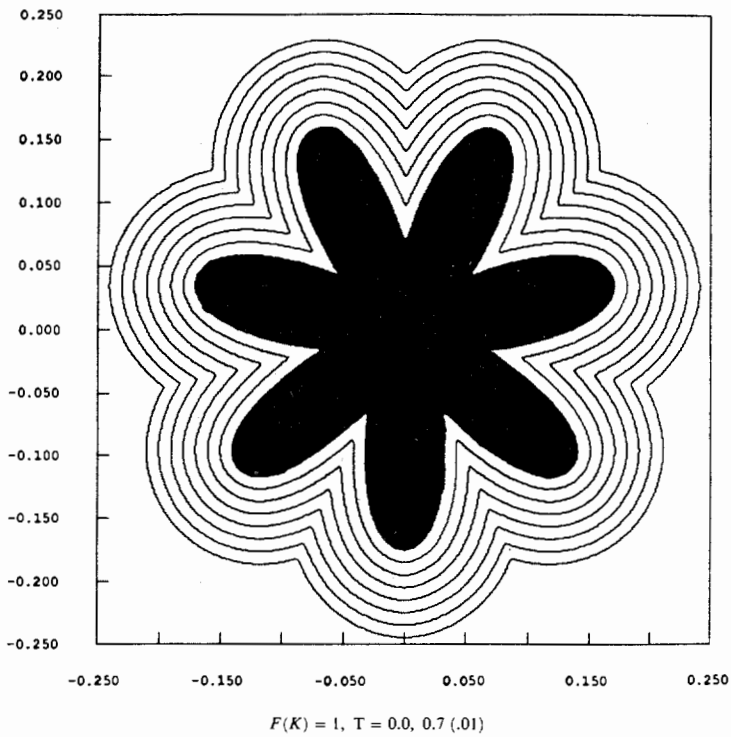

FIGURE 9. Star-shaped front burning out: $F(K) = 1$. (Reprinted from [24])

wound spiral traced out by

$$\gamma(0) = (0.1e^{(-10y(s))} - (0.1 - x(s))/20)(\cos(a(s)), \sin(a(s))), \qquad s \in [0, 1],$$

where $a(s) = 25\tan^{-1}(10y(s))$ and

$$(x(s), y(s)) = ((0.1)\cos(2\pi s) + 0.1, (0.5)\sin(2\pi s) + 0.1).$$

We choose 200 mesh points and $\Delta t = 0.0001$. Here, we have rescaled time by a factor of 100 because the real front moves so quickly. In Figures 10a–d we show the unwrapping of the spiral, the collapse to a circle, and the eventual disappearance at $t = .295$. Note that we are following a family of nested initial spirals lying on the higher-dimensional surface. The particular front we are interested in vanishes when the evolving surface moves entirely above the xy-plane, that is, when $\Psi_{ij}^n > 0$ for all ij.

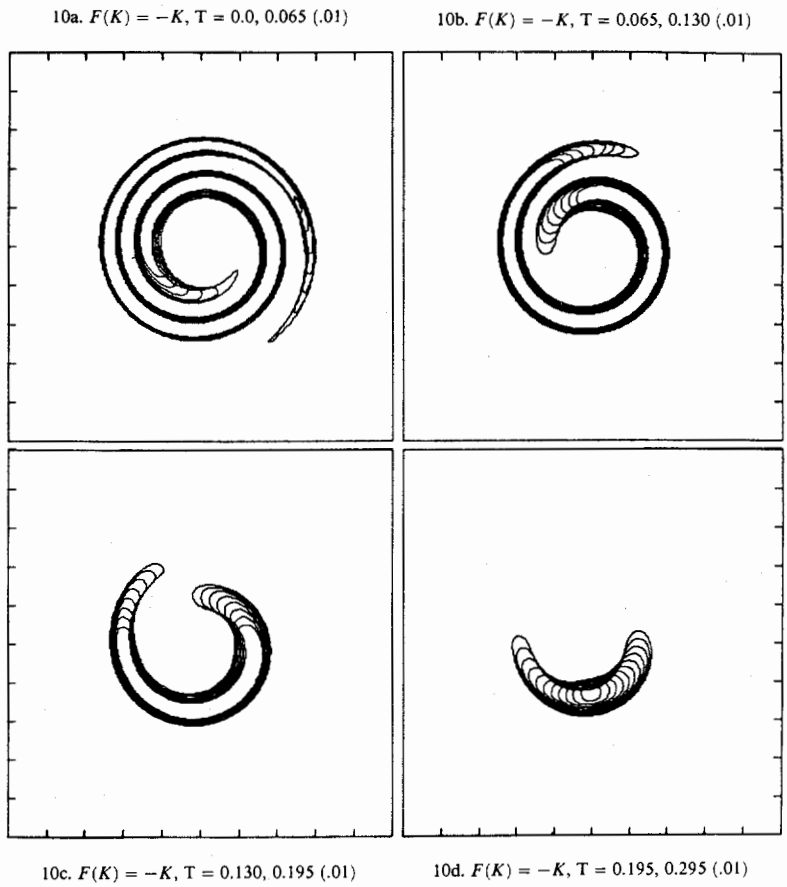

FIGURE 10. Wound spiral collapsing under curvature: $F(K) = -K$. (Reprinted from [24])

Burning spiral and change of topology: Merging and breaking. Suppose the wound spiral in the previous example represents the boundary of a flame burning with speed $F(K) = 1 - \varepsilon K$, $\varepsilon = .01$. We use 200 mesh points per side and $\Delta t = .0001$. Figure 11a shows the initial curve as the boundary of the shaded region. In Figure 11b, the spiral expands and pinches off due to the outward normal burning, separating into two flame fronts, one propagating outwards and one burning in. In Figure 11c, the front at $t = .04$ is the boundary of the shaded region. The outer front

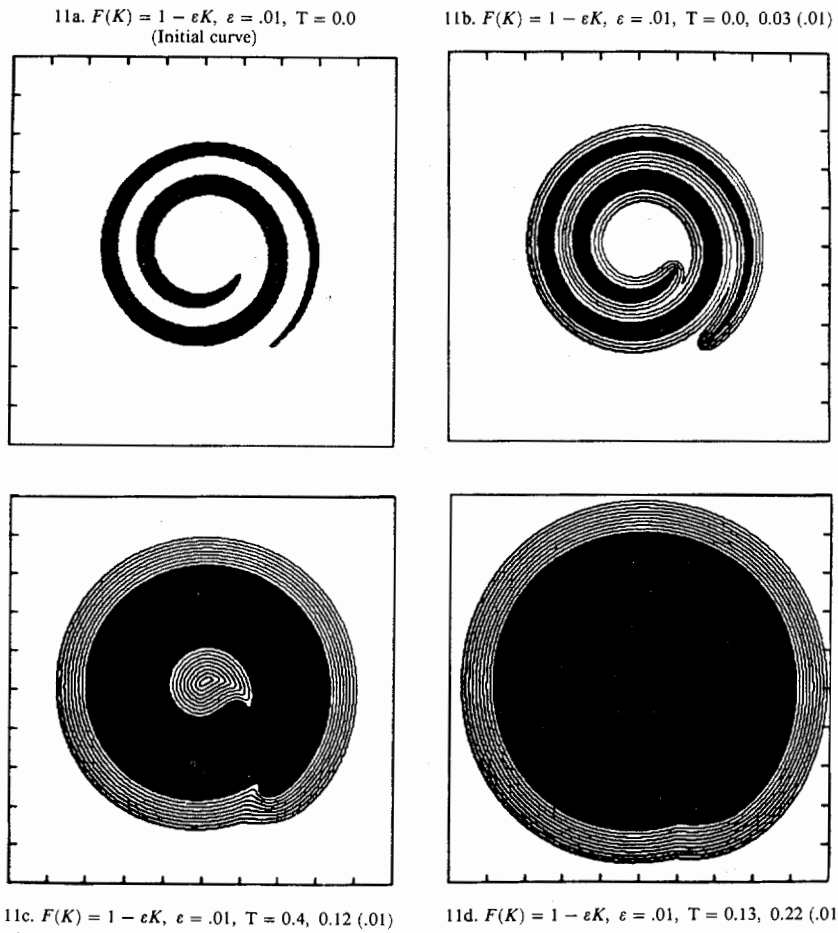

FIGURE 11. Burning spiral: Merging and breaking $F(K) = 1 - \varepsilon K$, $\varepsilon = .01$. (Reprinted from [24])

expands and the inner front collapses and disappears. In Figure 11d, all that remains is the outer front which asymptotically approaches a circle.

Burning torus: Change of topology, merging and breaking, $F(K) = 1 - \varepsilon K$, $\varepsilon = .01$. We evolve the toroidal initial surface, described by the set of all points (x, y, z) satisfying

$$z^2 = (0.5)^2 - ((x^2 + y^2)^{1/2} - 0.05)^2.$$

This is a torus with main radius .5 and smaller radius .05. The computational domain is a rectangular parallelepiped with lower left corner

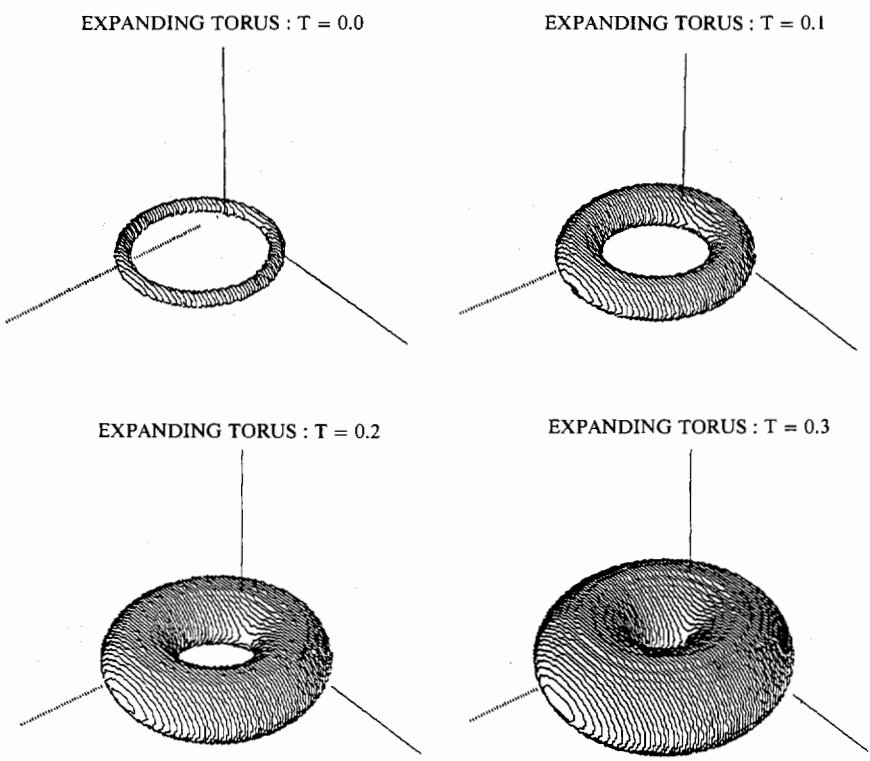

12a. $F(K) = 1 - \varepsilon K$, $\varepsilon = .01$, Surface at T = 0.0, 0.1, 0.2, 0.3

FIGURE 12. Burning torus: Change of topology, $F(K) = 1$ (Beginning). (Reprinted from [24])

$(-1, -1, -0.8)$ and upper right corner $(1, 1, 0.8)$. We evolve the surface with $F(K) = 1 - \varepsilon K$, $\varepsilon = .01$, $\Delta = .01$, and 90 points per x and y side of the domain and 72 mesh points in the z direction. Physically, we might think of this problem as the boundary of a torus separating products on the inside from reactants outside, with the burning interface propagating outwards. We follow a nested set of concentric toroidal shapes, and look for the level surface $\psi(x, y, z, t) = 0$. In Figure 12 (a and b), we plot this surface at various times. First, the torus burns smoothly (and reversibly) until the inner radius collapses to zero. At the time ($T = 0.3$), normals collide, the topology changes, and the entropy condition is automatically invoked. The surface then looks like a sphere with deep inward spikes

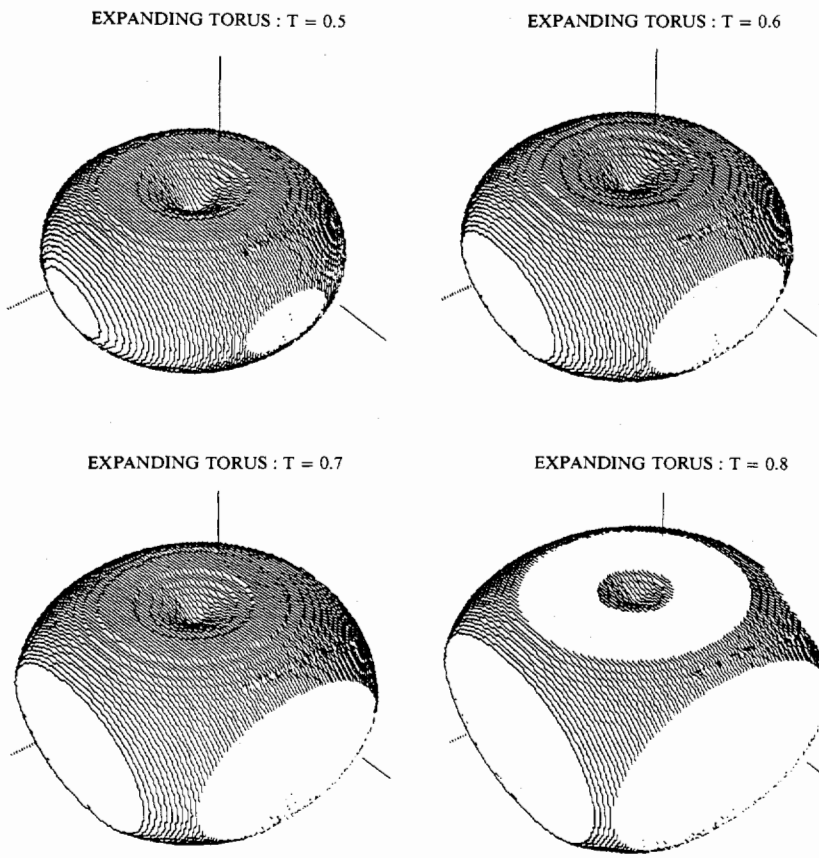

12b. $F(K) = 1 - \varepsilon K$, $\varepsilon = .01$, Surface at T = 0.5, 0.6, 0.7, 0.8

FIGURE 12. Burning torus: Change of topology, $F(K) = 1$ (Continued).

at the top and bottom which open up as the surface asymptotically approaches a sphere. Note that in the final four figures, the boundary of the expanding torus intersects the edge of the computational domain. This is reflected in the slicing of the level surface $\psi = 0$ by the sides of the box. This demonstrates the advantage of an upwind formulation, since information flows out of the computational box.

Collapse of torus under its mean curvature: $F(K) = -K$. Next, we compute the motion of a torus under its mean curvature. This problem has been studied in [1], [15], [16]. The inner radius is .25 and the outer

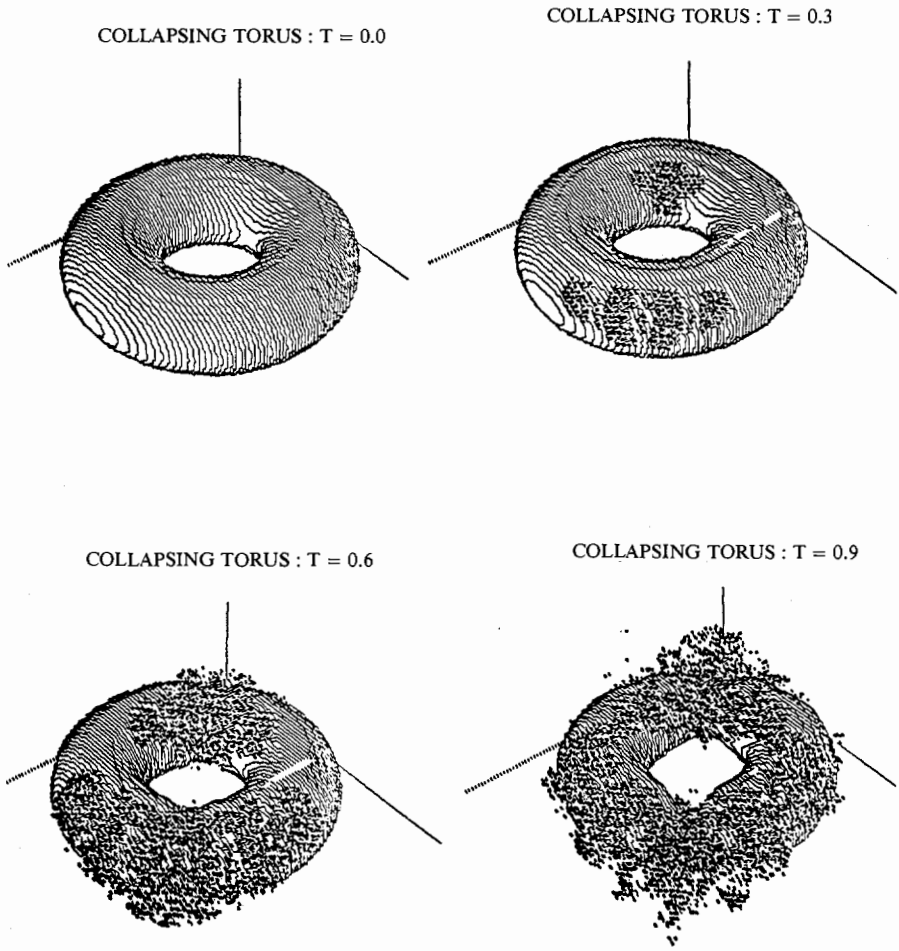

13a. $F(K) = -K$, Surface goes unstable, T = 0.0, 0.3, 0.6, 0.9

FIGURE 13. Collapse of torus under mean curvature (Beginning) Instability results from too large a time step ($\Delta t = .05$). (Reprinted from [24])

radius is .5. We embed the problem in a unit cube of side length 2, and use a fairly coarse mesh with 45 points per side.

First, we perform the calculation with time step $\Delta t = .05$. Again, time is rescaled by a factor of 100 because the flow proceeds so quickly. Soon after the front starts to collapse, the calculation goes unstable, (see Figure

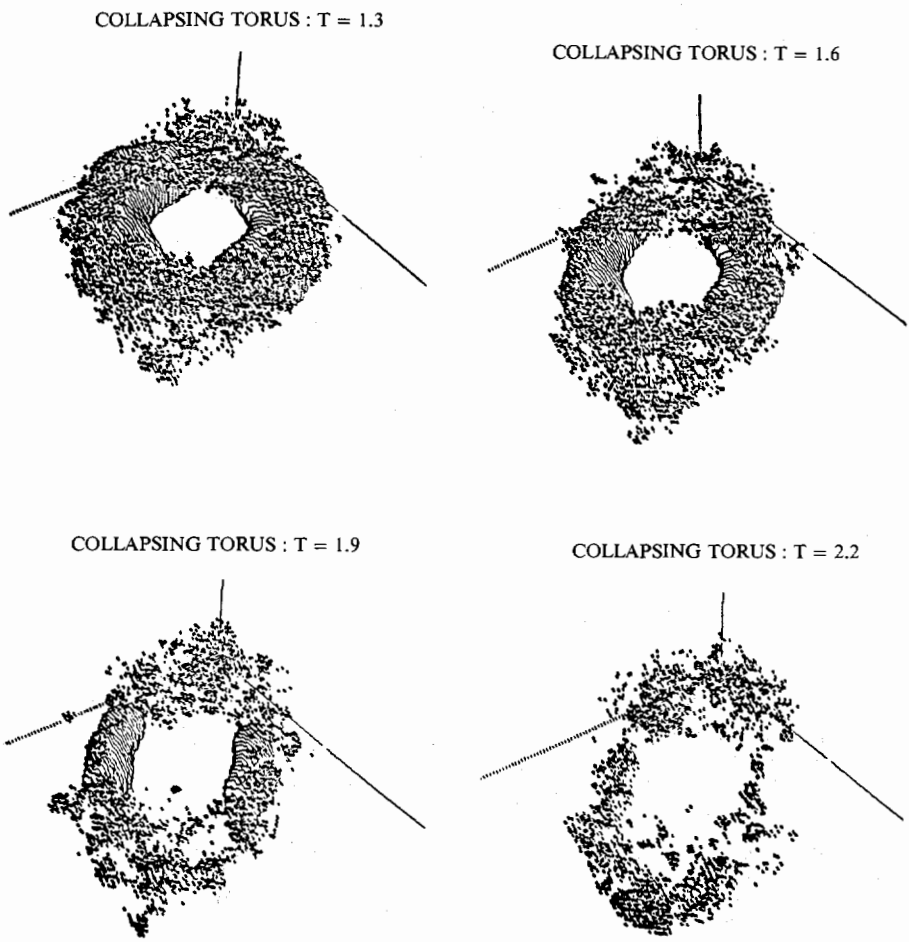

13b. $F(K) = -K$, Surface continues unstable, T = 1.3, 1.6, 1.9, 2.2

FIGURE 13. Collapse of torus under mean curvature (Continued)
Instability results from too large a time step ($\Delta t = .05$)

13). This is manifested by the contour plotter finding numerous small spheres of radius one cell size having value $\psi = 0$. As time progresses, the evolving surface degenerates into noise as the contour plotter desperately tries to find zero level surfaces of a wildly oscillating function. What has

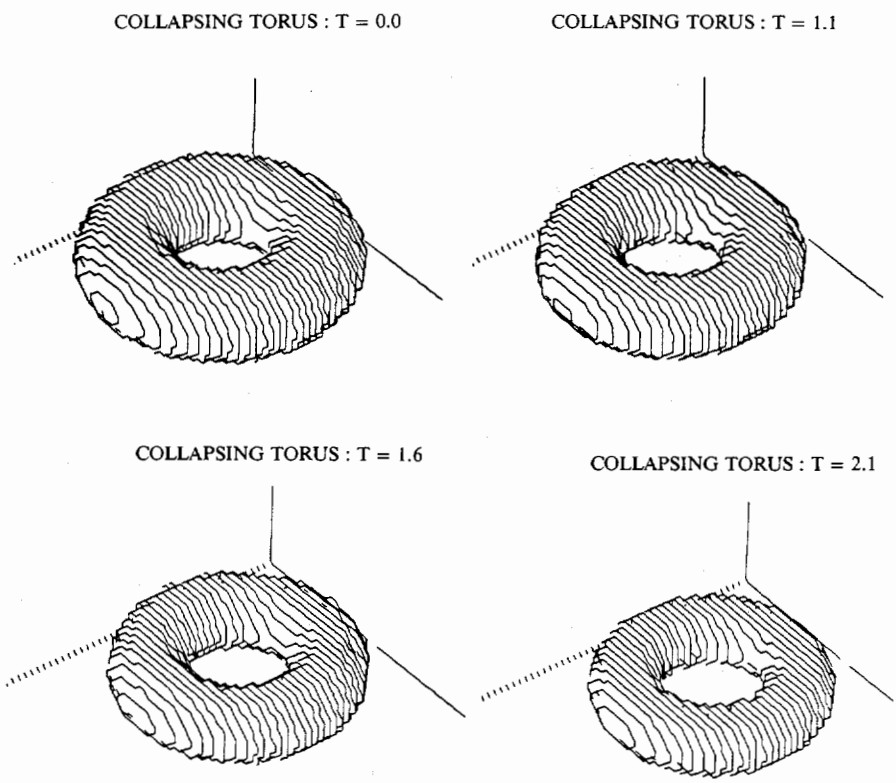

14a. $F(K) = -K$, Stable collapse, T = 0.0, 1.1, 1.6, 2.1

FIGURE 14. Collapse of torus under mean curvature (Beginning) Stable collapse ($\Delta t = .01$). (Reprinted from [24])

happened is that we have violated the stability criteria for our numerical algorithm.

However, because the grid size is fixed, we need only decrease the time step to satisfy stability. This is one of the strongest arguments for an Eulerian formulation. In Figures 13a and 13b, we repeat the calculation with time step $\Delta t = .01$. The torus deflates smoothly and collapses to the ring shown at $T = 4.1$ before it vanishes. The final shape shown is the smallest surface that can be resolved on the given mesh size.

Collapse of a dumbbell under its mean curvature: Change of topology. Recently, there has been considerable interest in the collapse of a closed, nonconvex, hypersurface in R^3 (for example, see [15], [16]) moving by

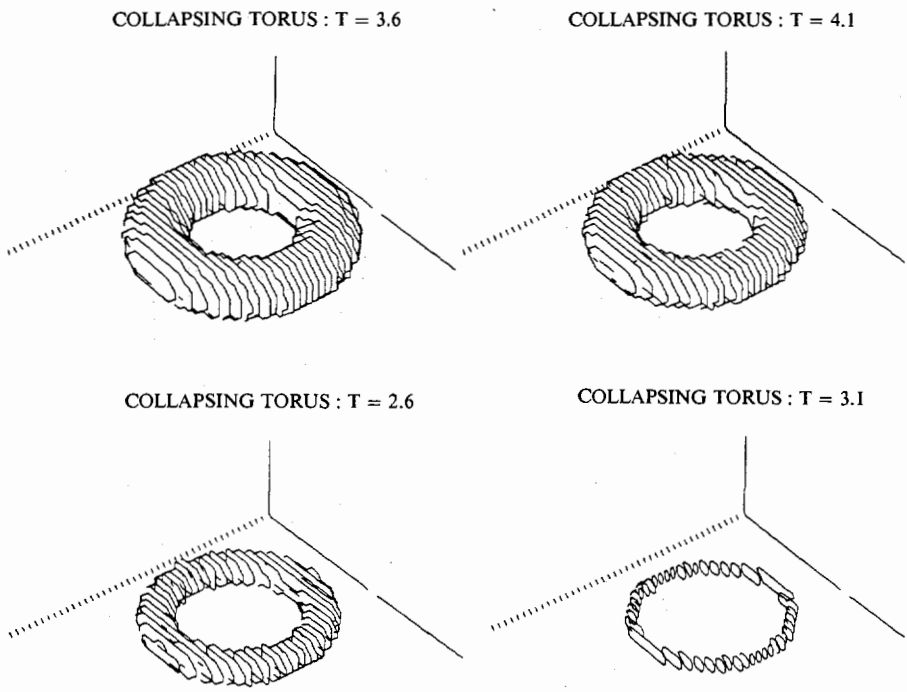

14b. $F(K) = -K$, Continued stable collapse, T = 2.6, 3.1, 3.6, 4.1

FIGURE 14. Collapse of torus under mean curvature (Continued)
Stable collapse ($\Delta t = .01$)

its mean curvature. In our final example, we use the above algorithms to study the motion of a dumbbell as it shrinks. Consider the dumbbell made up of two spheres, each of radius .3, and connected by a cylindrical handle of radius .15 (see Figure 15). The x-axis is the axis of symmetry. We wish to follow the evolution of this surface as it moves under its mean curvature.

We must be slightly careful in setting up the problem. Our algorithm computes the curvature at each mesh point by evaluating the expression for the mean curvature, namely

$$K = \frac{\begin{bmatrix} (\psi_{yy}(\psi_x^2 + \psi_y^2) + \psi_{xx}(\psi_y^2 + \psi_z^2) + \psi_{zz}(\psi_x^2 + \psi_y^2) \\ -2\psi_x\psi_y\psi_{xy} - 2\psi_x\psi_z\psi_{xz} - 2\psi_y\psi_z\psi_{yz}) \end{bmatrix}}{(\psi_x^2 + \psi_y^2 + \psi_z^2)^{3/2}}$$

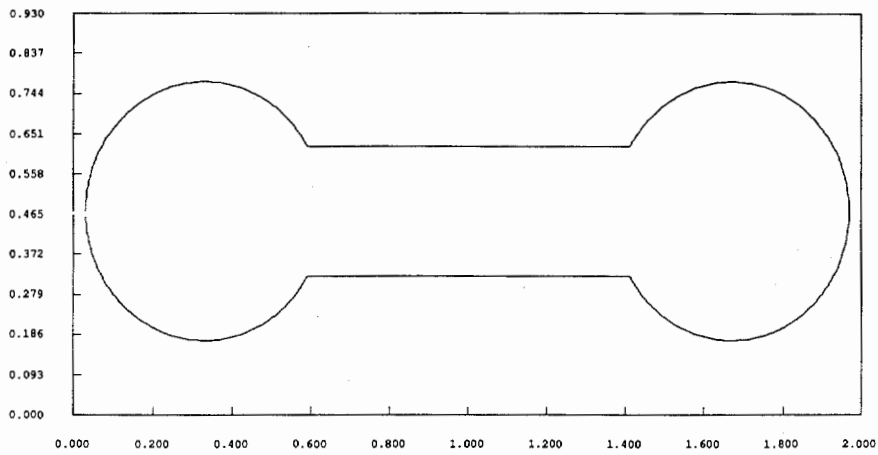

FIGURE 15. Initial shape of dumbbell

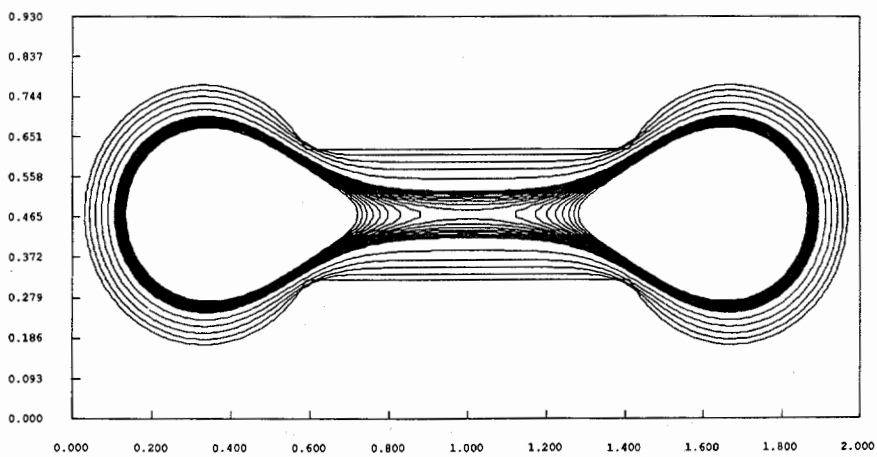

FIGURE 16. $F(K) = -K$: $214 \times 72 \times 72$ Grid

Both the numerator and denominator vanish at the center of this dumbbell. Evaluation of this ratio causes the computer code to halt. Formally speaking, whenever this occurs we should insert the correct limiting form of the expression $F(K)\nabla\psi$ into our algorithm. Unfortunately, the correct limiting form is a point of controversy, and one wants to avoid building

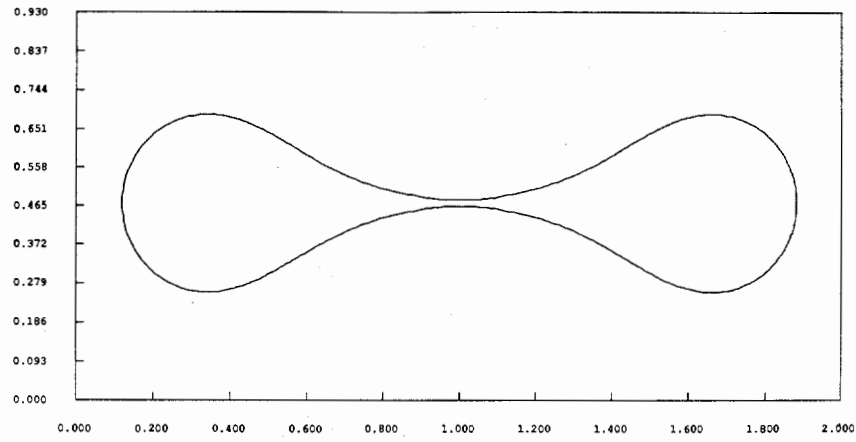

FIGURE 17. $F(K) = -K$: Final shape reached on $214 \times 72 \times 72$ grid before break

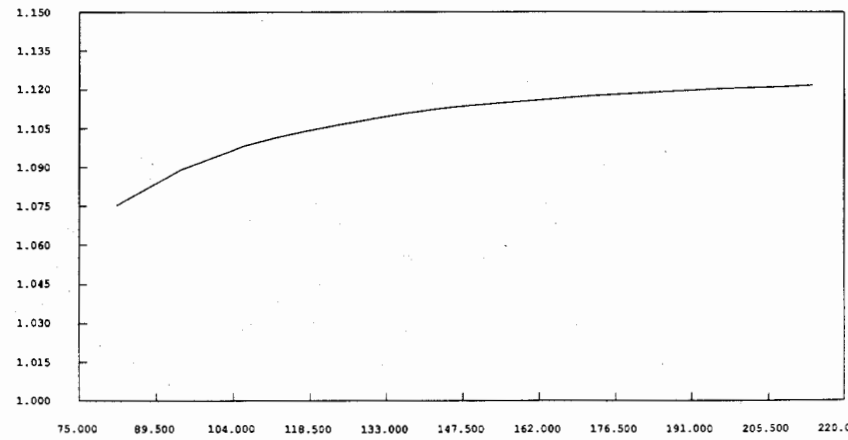

FIGURE 18. Time until singularity vs. Number of mesh points in x direction

into the code an a priori assumption about the behavior of the figure where the singularity occurs. We circumvent this problem by using an even number of grid points in all three coordinate directions x, y, and z, so that points are staggered around the center axis of rotation. Thus, by avoiding symmetries with this placement of grid points, the denominator does not vanish. We performed a calculation with 214 grid points in the x direction, and 72 grid points in both the y and z directions. The computational

box stretched from -1.0 to 1.0 in the x direction, and $-1/3$ to $1/3$ in both the y and z directions. We chose a time step of $\Delta t = .0002$.

The results of our calculation are shown in Figure 16. We show a diagonal cross-section of the dumbbell (that is, the intersection of the moving surface with the plane $y = z$). Although the initial shape is only piecewise continuous, the corners are immediately smoothed out as the surface moves inward. The position of the front is plotted every 100 time steps until the handle becomes small, and then every 10 time steps. The figure shows the narrowing of the handle as the surface shrinks, and the break into two distinct pieces each of which collapses to a point.

In Figure 17, we show the final shape of surface obtained on a $214 \times 72 \times 72$ grid before it separates into two pieces. From this drawing, one can get a sense of the size of the mesh used in the calculation. The narrow throat at the center is little wider than $\sqrt{2}$ times the length of one mesh cell (the factor $\sqrt{2}$ comes from the fact that we are looking at a cross-section obtained by intersecting the moving surface with the plane $y = z$).

It is important to verify that our calculations are unchanged under refinement of numerical parameters. We performed 23 separate calculations of the collapsing dumbbell using meshes with $82, 88, 94, \cdots, 208, 214$ points in the x direction, always maintaining a 3 : 1 ratio between the number of mesh points in the x direction and the number in the y and z directions. In each calculation, the dumbbell shrank, the neck pinched off, and the surface separated into two pieces which continued to collapse. As a final check, in Figure 18, we plot the time until the singularity develops against the number of mesh points on the x axis. The results are robust; as the mesh is refined the curve quickly levels off and little change is seen in the singularity time.

An interesting issue is the type of singularity (i.e., a corner or a cusp) that develops. It is not clear from our preliminary calculations which occurs as the topology changes. A careful numerical study would require many more grid points and a higher order accurate method, such as those developed in [24]. The number of grid points used in the above calculation ($214 \times 72 \times 72$) is close to the maximum number that can be stored easily in the memory of a Cray 1 with no memory-saving tricks. Further attempts to investigate the nature of the singularity might employ uneven meshes, multi-grid schemes, and a judicious use of symmetry properties of the evolving shape.

Acknowledgments. The Hamilton-Jacobi algorithm used in these calculations is joint work with S. Osher. In addition, valuable comments were provided by M. Grayson and O. Hald.

All calculations were performed at the University of California, Berkeley, and the Lawrence Berkeley Laboratory.

References

[1] K. A. Brakke, *The motion of a surface by its mean curvature*, Princeton University Press, Princeton, NJ, 1978.

[2] A. J. Chorin, *Flame advection and propagation algorithms*, J. Comput. Phys. **35** (1980) 1.

[3] ——, *Curvature and solidification*, J. Comput. Phys. **58** (1985) 472.

[4] M. G. Crandall & P. L. Lions, *Viscosity solutions of Hamilton-Jacobi equations*, Trans. Amer. Math. Soc. **277** (1983) 1.

[5] B. Engquist & S. Osher, *Stable and entropy satisfying approximations for transonic flow calculations*, Math. Comp. **34** (1980) 45.

[6] B. Engquist & S. Osher & R. Sommerville, *Large-scale computations in fluid mechanics*, Vols. I and II, Lectures in Applied Math., Amer. Math. Soc., Providence, RI, 1985.

[7] C. L. Epstein & M. I. Weinstein, *A stable manifold theorem for the curve shortening equation*, Comm. Pure Appl. Math. **40** (1987) 119.

[8] M. L. Frankel & G. I. Sivashinsky, *The effect of viscosity on hydrodynamic stability of a plane flame front*, Comb. Sci. Tech. **29** (1982) 207.

[9] M. Gage, *An isoperimetric inequality with applications to curve shortening*, Duke Math. J. **50** (1983) 1225.

[10] ——, *Curve shortening makes convex curves circular*, Invent. Math. **76** (1984) 357.

[11] M. Gage & R. S. Hamilton, *The equation shrinking convex planes curves*, J. Differential Geometry **23** (1986) 69.

[12] J. Glimm, *Solutions in the large for nonlinear hyperbolic systems of conservation laws*, Comm. Pure Appl. Math. **18** (1965) 697.

[13] S. K. Godunov, *Finite difference method for numerical computation of discontinuous solutions of the equations of fluid mechanics*, Mat. Sb. **47**, (1959) 271.

[14] M. Grayson, *The heat equation shrinks embedded plane curves to round points*, J. Differential Geometry **26** (1987) 285.

[15] ——, *A short note on the evolution of a surfaces via mean curvature*, preprint, Department of Mathematics, Stanford University, 1987.

[16] G. Huisken, *Flow by mean curvature of convex surfaces into spheres*, J. Differential Geometry **20** (1984) 237.

[17] L. Landau, *On the theory of slow combustion*, Acta Physiocochimica URSS **19** (1944) 77.

[18] J. S. Langer, *Instabilities and pattern formation in crystal growth*, Rev. Modern Phys. **52** (1980) 1.

[19] J. S. Langer & H. Muller-Krumhaar, *Mode selection in a dendrite-like nonlinear system*, Phys. Rev. A **27** (1983) 499.

[20] P. D. Lax, *Weak solutions of nonlinear hyperbolic equations and their numerical computations*, Comm. Pure Appl. Math. **7** (1954) 159.

[21] G. H. Markstein, *Experimental and theoretical studies of flame front stability*, J. Aero. Sci. **18** (1951), 199.

[22] ——, *Non-steady flame propagation*, Pergamon Press and MacMillan, New York, 1964.

[23] O. A. Oleinik, *Discontinuous solutions of nonlinear differential equations*, Trudy Moscow Mat. Obsc. **5** (1956) 433.
[24] S. Osher & J. A. Sethian, *Fronts propagating with curvature-dependent speed: Algorithms based on Hamilton-Jacobi formulations*, J. Comput. Phys. **79** (1988) 12–49.
[25] B. R. Pamplin, *Crystal growth*, Pergamon Press, New York, 1975.
[26] J. Rubinstein, P. Sternberg & J. B. Keller, *Fast reaction, slow diffusion, and curve shortening*, preprint, Department of Math., Stanford University, 1987.
[27] J. A. Sethian, *An analysis of flame propagation*, Ph.D. Dissertation, University of California, Berkeley, 1982; CPAM Rep. 79.
[28] ——, *Curvature and the evolution of fronts*, Comm. Math. Phys. **101** (1985) 487.
[29] ——, *Numerical methods for propagation fronts*, in Variational Methods for Free Surface Interfaces (P. Concus and R. Finn, eds.), Springer, New York, 1987.
[30] J. A. Sethian & S. Osher, *Hamilton-Jacobi based algorithms for interface-media interactions*, J. Comput. Phys., to be submitted.
[31] G. I. Sivashinsky, *Nonlinear analysis of hydrodynamic instability in laminar flames.* I, Acta Astronautica, **4** (1977) 1177.
[32] G. Sod, *Numerical methods in fluid dynamics*, Cambridge University Press, New York, 1985.
[33] D. Turnbull, *Phase changes*, in Solid State Physics. 3 (F. Sietz and D. Turnbull, eds.), Academic Press, New York, 1956.
[34] Y. B. Zeldovich, *Structure and stability of steady laminar flame at moderately large Reynolds numbers*, Comb. Flame **40** (1981) 225.

UNIVERSITY OF CALIFORNIA, BERKELEY